



New criterion for achieving efficient flow fields in PEM fuel cells

Mazaher Rahimi-Esbo^{a,*} | Kamran Dadashi Firouzjaei^a | Mehran Ghasemian^b

^a Northern Research Center for Science & Technology, Malek Ashtar University of Technology, Iran

^b Faculty of Mechanical Engineering, Babol Noshirvani University of Technology, Babol, Iran

* Corresponding author, Email: mr Rahimi@mut.ac.ir

Article Information

Article Type

RESEARCH ARTICLE

Article History

RECEIVED: 12 Oct 2023

REVISED: 03 Dec 2023

ACCEPTED: 25 Dec 2023

PUBLISHED ONLINE: 02 Jan 2024

Keywords

PEM fuel cell

Water management

Gas flow field

Performance evaluation criteria

Abstract

Due to the needs of industries for clean and environmentally friendly fuels today, new energy sources such as fuel cells are at the center of attention. Polymer fuel cells, meanwhile, require a short start-up time due to low operating temperature, high power density, no emission and very low noise, making them the best option for vehicles as an alternative to internal combustion engines. One of the most important reasons for fuel cell loss is the uneven distribution of reactants on the active area, which causes non-uniform reactions. Therefore, the use of an optimal flow field to improve the durability and performance of PEM fuel cells seems necessary. Although different studies introduced novel designs, a study comparing different patterns comprehensively to introduce the best ones is not performed yet. In this study, first, a numerical validation was performed with an experimental test that showed good accuracy. Then, to achieve efficient patterns, several flow field designs were inspired by previous effective designs and others were selected as superior designs from the literature. The effects of presented geometries on the performance of a PEMFC were investigated to improve its performance. In addition, efficient evaluation criteria from the literature were employed to better analyze the performance of such systems, and the ones consistent with the I-V performance were introduced. By surveying the criteria, a novel performance factor was introduced that showed the best agreement with the I-V performance. The results were obtained in single-phase and two-phase approaches, which lead to remarkable findings. The two-phase study revealed that the waved serpentine case has the highest electrical performance with the highest mass fraction of oxygen.

Cite this article: Rahimi-Esbo, M., Dadashi Firouzjaei, K., Ghasemian, M. (2024). New criterion for achieving efficient flow fields in PEM fuel cells. DOI: 10.22104/HFE.2024.6696.1288



© The Author(s).

Publisher: Iranian Research Organization for Science and Technology (IROST)

DOI: 10.22104/HFE.2024.6696.1288

1 Introduction

With increasing attention to fossil fuels independency and environmental concerns, alternative fuel resources have attracted much attention. In order to find more efficient and cleaner energy generation methods, fuel cells have been introduced as a suitable option. Fuel cells operate on the principle of direct energy conversion and use electrochemical reactions to generate electricity in one step via the chemical potential of a fuel. There are different types of fuel cells, among which polymer membrane fuel cells showed better performance due to lower operating temperature, fast start-up, and silent operation. A schematic of a common polymer membrane fuel cell is shown in Figure 1.

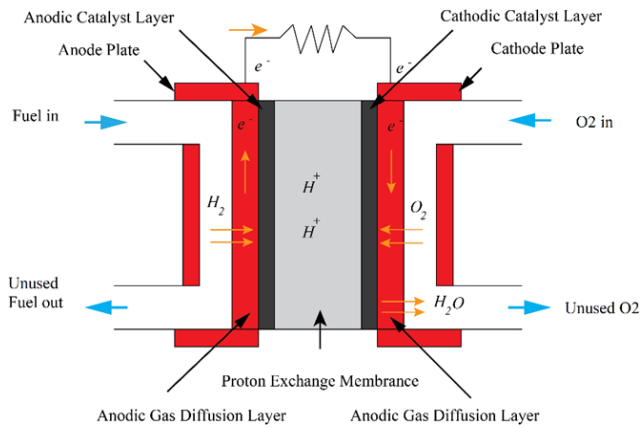


Fig. 1. Schematic of a PEM fuel cell.

Various studies have been carried out, especially in the field of gas flow fields of polymer membrane fuel cells, which shows the importance of this issue and also indicates that it can still be an active area for research and development of this type of fuel cell. Several review studies have been performed on different kinds of flow fields and their effect on PEM fuel cells in recent years. In 2012, Menso et al. [1] investigated the effect of geometric parameters of flow fields on fuel cell performance. Kahraman and Orhan [2] comprehensively reviewed configurations of currently available flow fields and provided step-by-step modeling of an optimal flow field design.

Lim et al. [3] then studied the effect of flow fields with different designs on water management and distribution of reactants in such systems. Further, in a numerical study [4], they examined the effect of flow fields with modified parallel designs. The performance of novel flow fields was evaluated from the perspective of reactants distribution, temperature uniformity and current density production, which showed the superiority of the design. In a numerical study conducted

by Shen et al. [5], the synergy criterion based on the improved mass transfer theory was introduced and applied to the flow field. They compared the performance of a flow field with four obstacles in the path with that of a conventional serpentine channel. They found that by adding obstacles, the mean synergy angle between the gas velocity and the concentration gradient at the cathode decreased, while the effective mass transfer coefficient increased, resulting in improved cell performance.

A numerical study by Rostami et al. [6] proposed a three-dimensional model to investigate the effect of bend size of serpentine channels on the performance of the polymer membrane fuel cell. The results showed that by increasing the bend size from 1 to 1.2 mm, not only does the overpotential decrease but also the temperature gradient diminishes. Moreover, the serpentine channel with the bend size of 1.2 mm is successful in preventing internal secondary flow and causes performance improvement up to 90%, compared to the case with the bend size of 0.8 mm. Ramin et al. [7] in a numerical study introduced the channel design with traps and optimized the number and length of traps in the channel path. The proposed design dramatically increases the current density while its manufacturing process is as simple and inexpensive as direct conventional channels.

Singdeo et al. [8] proposed a modified serpentine flow field design to be used in polymer fuel cells, and by modifying the flow field paths, they were able to increase the current density in addition to increasing the uniformity of the distribution of the reactants. Baz et al. [9] conducted a numerical study and presented several new serpentine channels in order to uniformly distribute the reactants on the active area, increase the under rib mass transport, reduce flooding on the interface between the gas diffusion layer and the catalyst layer and keep the membrane water content in the appropriate range for better proton conductivity. The novel designs were achieved based on variations of three factors, including the flow distribution path, the number of paths, and the rib length. The results revealed that a 22.6% increase in power density is achievable in the most optimal case.

A new reduction design for the gas channels of PEM fuel cells was proposed by Alizadeh et al [10]. They first described the new design and then optimized its geometric parameters. It was observed that the new design could provide a uniform distribution of reactants and water. Li et al. [11] introduced the waved serpentine design for use in the flow fields. They proved that it can improve the transport of reactants and cell performance by periodic changes in channel depth. Also, a lower pressure drop was observed using the new de-

sign. The numerical results obtained in this study were confirmed by experimental results.

Ashrafi et al. [12] investigated the improvement of two-phase flow uniformity in polymer fuel cells. First, experiments were performed to find the appropriate stoichiometric ratio for the cathode, water coverage rate and fuel cell power density with a Z-type flow field. Then, using a 3D model, a modified flow field with uniform distribution of single-phase and two-phase flows was introduced.

In two studies by Heidari et al. [13, 14], first the effect of in-line and staggered obstacles in a parallel flow field was examined in an experimental study and then the effect of the number, height and direction of obstacles placed in the flow channel was investigated numerically. The results of the experimental research showed that in the staggered configuration due to under rib mass transport compared to the in-line mode where only mass transportation occurs under the obstacle, the cell performance enhances up to 28% compared to the simple parallel channel and 18% compared to the in-line obstacle configuration.

Wen et al. [15] introduced the intersectant flow field. With the help of CFD, they obtained optimal values of 0.3 and 0.5 mm for channel depth and porosity of this type of channel and then compared the results with the serpentine channels in experiments and found that the advantages of this novel design are in higher reaction rate and uniformity and better water removal rate.

The main challenges for PEM fuel cell systems are the creation of hot spots and flooding, which can be due to the uneven distribution of reactants in the anodic and cathodic flow channels. Such phenomena reduce the performance of the system. The flooding phenomenon in the cathode, which occurs due to the accumulation of liquid water in the pores of the catalyst layer, micro-porous layer and gas diffusion layer, is one of the main performance-reducing parameters caused by oxygen not reaching the catalyst and membrane surface; it is the most common problem in heat and water management processes. The flooding in channels can be managed by controlling the evaporation and condensation processes, which are strongly dependent on the temperature distribution at the cell surface [16–18]. Since the fabrication and testing of polymer fuel cells are very time-consuming and costly, computational fluid dynamics can play an important role in accurately analyzing the phenomena governing the whole system, which are difficult and sometimes impossible to analyze with conventional experimental methods.

Although many studies tried to improve available flow fields and introduce novel efficient flow-field de-

signs, there is a lack of a study to compare different types of designs and introduce applicable evaluation criteria to help researchers find optimum flow fields based on the user needs. Most of the studied literature introduced a limited number of efficient flow fields. However, in this study first, new flow field patterns are presented, and then, the performance of efficient channel designs among the literature are compared deliberately. Although some evaluation criteria have been introduced to the literature, there is a lack of an analytical comparison of the efficient criteria in order to find applicable ones. Hence, the performances of efficient flow fields are compared using different evaluation criteria. In addition, by evaluating the effective parameters and analyzing the performances of different patterns, a novel factor is introduced here as a useful tool to help users choose the pattern with the highest performance.

2 Geometries and computational domain

2.1 Flow field designs

In this section, novel and selected gas flow fields were presented based on the conducted research on various efficient flow fields among the literature, after the initial analysis of the designs performed to select the best samples. After selecting the fitting designs, the design modeling, meshing and implementation of selected cases were carried out in order to compare them with the aim of finding the best option. The flow field designs analyzed in this study are chosen based on or inspired by studies from the state-of-the-art literature, each of which showed good performance in various functional fields such as good reactant distribution, low pressure drop, uniform temperature distribution and high current density. The selected channel designs in the present study include the following designs, a schematic view of which is shown in [Figure 2](#).

- I. Double channel serpentine, as a base serpentine design;
- II. Double channel serpentine (bend size 1.2 mm), inspired by the design of Rostami et al. [6];
- III. Double channel serpentine with trap, inspired by the design of Ramin et al. [7];
- IV. Modified parallel (channel size 3 mm), inspired by the design of Lim et al. [4];
- V. Modified parallel (channel size 2 mm) [4];
- VI. Modified serpentine, from Singdeo et al. [8];
- VII. Reduction, from Alizadeh et al. [10];
- VIII. Waved serpentine, from Li et al. [11].

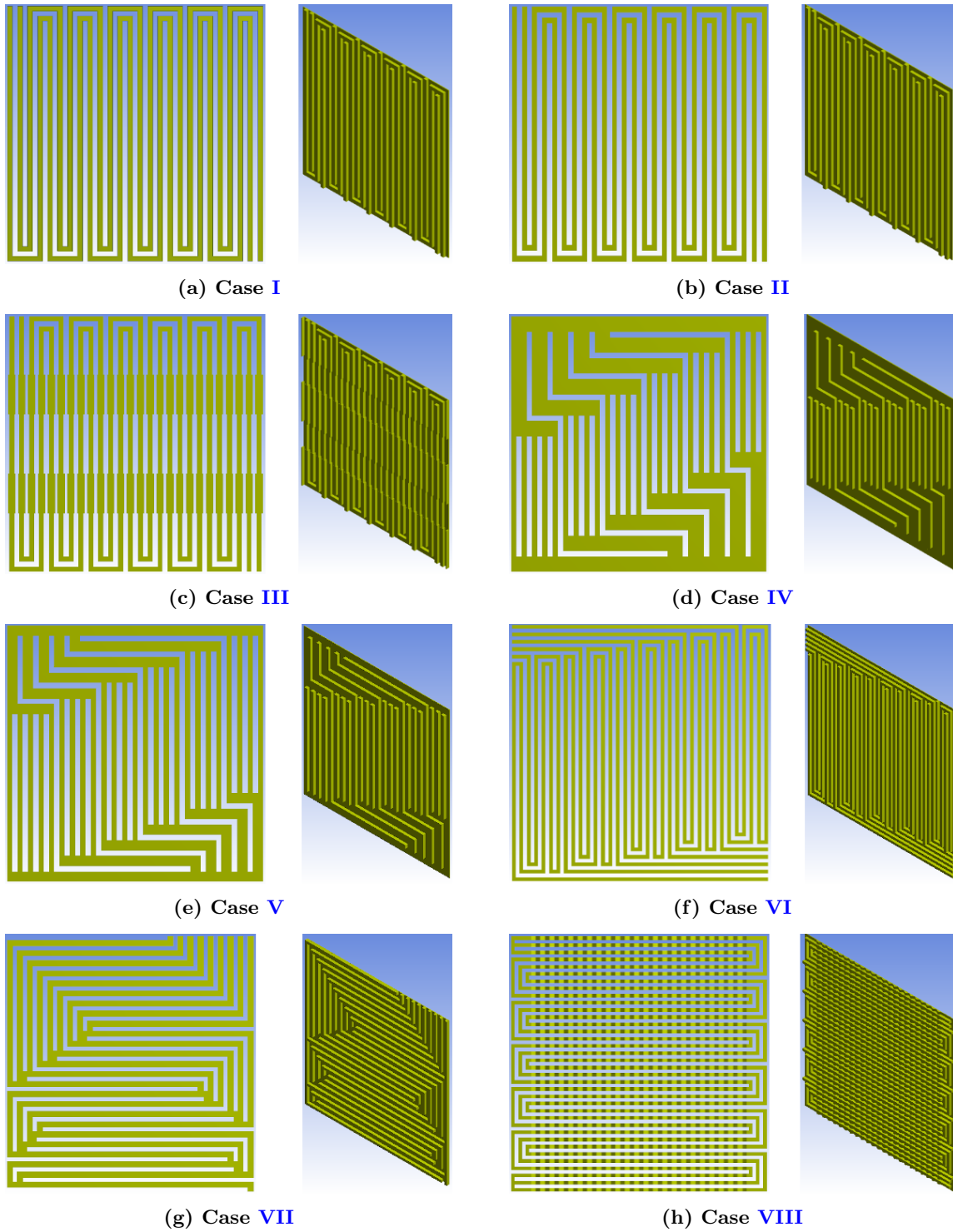


Fig. 2. Perspective and front view of selected flow field designs (cases I to VIII).

2.2 Computational domain

A schematic of the computational domains, dimensions, and boundary conditions applied to a numerical sample of a double channel serpentine design is shown in Figure 3. This figure shows the position of inlets and outlets of the flow field as well as the dimensions of the

system components. In order to increase the accuracy of the analysis, the thickness of other parts of the PEM stack (except the flow channel) is considered the same. Further, the same designs are adopted for the anode and cathode flow channels, and the oxygen is used for the cathode inlets.

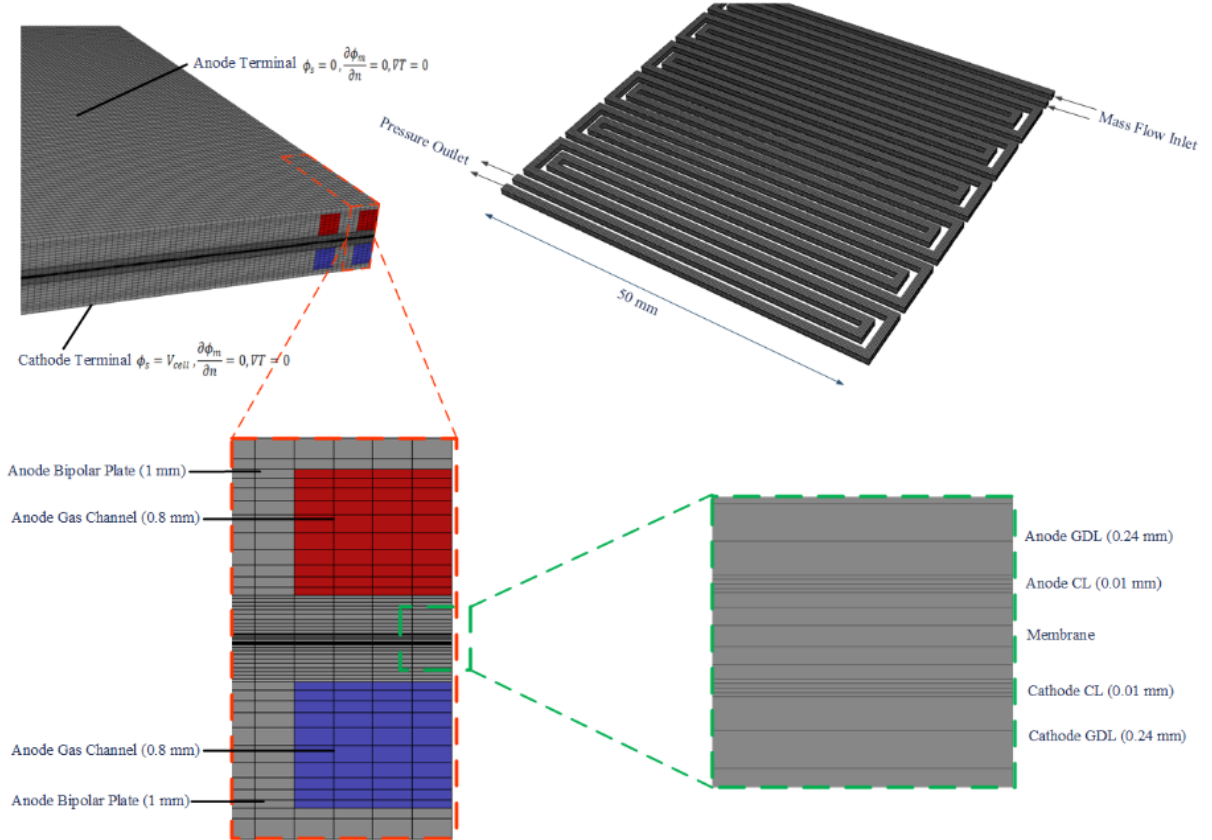


Fig. 3. A schematic of PEMFC and the computational domain.

3 Mathematical model

3.1 Governing equations

Generally, physical processes in a PEM fuel cell are explained mathematically by solving the mass, momentum, energy, electrochemical reactions, and charge transfer equations. For different layers and domains, suitable electrochemical equations with different source terms are solved numerically to obtain a system of equations for electrochemical and physical parameters to describe all the phenomena and their characteristics in a PEM fuel cell. Equations are derived by considering a laminar flow in isotropic porous regions. The

continuity equation is expressed as follows:

$$\nabla \cdot (\epsilon \rho_g \vec{V}_g) = -S_{\text{mass}} \quad (1)$$

The momentum equation of gas mixture species is defined as:

$$\frac{1}{(1-s)^2} \nabla \cdot (\epsilon \rho_g \vec{V}_g \vec{V}_g) = -\epsilon \nabla P_g + \frac{1}{1-s} \nabla \cdot (\epsilon \mu_g \vec{V}_g) + S_{\text{mom}} \quad (2)$$

In all equations, ϵ is the porosity coefficient, which is equal to one in the gas flow channels and a value between zero and one in the porous regions. Additionally, s is liquid saturation, μ_g is the viscosity of the gas mixture and S_{mom} is the momentum source term, which is

defined as follows [19].

$$S_{\text{mom}} = -\frac{\epsilon^2 \mu_g \vec{V}_g}{\kappa_p \kappa_{rg}} - \frac{\epsilon^3 C_f \rho_g}{\sqrt{\kappa_p}} |\vec{V}_g| \vec{V}_g, \quad (3)$$

where κ_p and κ_{rg} are permeability of the porous layer and relative permeability of the gas mixture, respectively.

The conservation of species participating in the reactions is achieved by [18]:

$$\nabla \cdot (\rho_g C_i \vec{V}_g) = \nabla \cdot (\rho_g D_i^{\text{eff}} \nabla C_i) + S_i, \quad (4)$$

where C_i is the mass fraction of each species, D_i^{eff} is the effective diffusivity and S_i is the species source term. The energy conservation equation can be explained as:

$$(\rho c_P)_{\text{eff}} (\vec{V}_g \nabla T) = \nabla \cdot k_{\text{eff}} \nabla T + S_{\text{temp}}, \quad (5)$$

in which $c_{P,\text{eff}}$ is the effective specific heat capacity, k_{eff} is the effective thermal conductivity and S_{temp} is the energy source term.

The transfer of electrons through the solid phase and the transfer of protons through the membrane is described by the equations of electric charge conservation as:

$$\begin{cases} \nabla \cdot (\sigma_s \nabla \phi_s) = S_{\text{es}}, \\ \nabla \cdot (\sigma_m \nabla \phi_m) = S_{\text{em}} \end{cases} \quad (6)$$

where σ_s and σ_m are the electrical conductivity in the solid phase and the ionic conductivity in the polymer membrane, respectively. In addition, ϕ_s and ϕ_m indicate the potentials of the solid and polymer membrane phases. The source terms S_{es} and S_{em} are called volumetric charge transfer. Theoretically, the activation loss η , which is the difference between the solid phase potential and the membrane, is the driving force of volumetric charge transfer. The electrical conductivity of solid materials is constant and depends on the properties of the material. But the ionic conductivity of the polymer membrane used in the model was calculated by Springer et al. [20]. The source terms for the solid and the membrane phase represent the production of electrons and protons, respectively, calculated by the Butler-Volmer equations [21]:

$$\begin{cases} j_{\text{an}} = j_{\text{an}}^{\text{ref}} \left(\frac{C_{\text{H}_2}}{C_{\text{H}_2}^{\text{ref}}} \right)^{\gamma_{\text{an}}} \\ \quad \times \left(\exp \left[\frac{\alpha_{\text{an}} F \eta_{\text{an}}}{RT} \right] - \exp \left[-\frac{\alpha_{\text{cat}} F \eta_{\text{an}}}{RT} \right] \right), \\ j_{\text{cat}} = j_{\text{cat}}^{\text{ref}} \left(\frac{C_{\text{O}_2}}{C_{\text{O}_2}^{\text{ref}}} \right)^{\gamma_{\text{cat}}} \\ \quad \times \left(\exp \left[-\frac{\alpha_{\text{cat}} F \eta_{\text{cat}}}{RT} \right] - \exp \left[\frac{\alpha_{\text{an}} F \eta_{\text{cat}}}{RT} \right] \right). \end{cases} \quad (7)$$

Source terms of electric charge conservation equations are called exchange current density. $j_{\text{an}}^{\text{ref}}$ and $j_{\text{cat}}^{\text{ref}}$ are exchange current density at the reference condition at the anode and cathode, respectively. F is Faraday's constant, C_i is the concentration of the species, C_i^{ref} is the concentration of the species at the reference conditions, and α_{an} and α_{cat} are anode and cathode transfer coefficients, respectively.

$$C_i = \frac{Y_i \rho_g}{M_i}. \quad (8)$$

The activation loss (η) at the anode and cathode is calculated as follows:

$$\begin{cases} \eta_{\text{an}} = \phi_s - \phi_m, \\ \eta_{\text{cat}} = \phi_s - \phi_m - V_{\text{oc}}, \end{cases} \quad (9)$$

where V_{oc} is the open-circuit voltage on the cathode side. Based on the conservation of the electric charge, the total current of electrons leaving the anode catalyst layer must be equal to the total current entering the cathode catalyst layer, as well as for the protons.

Liquid water saturation is defined as the volume ratio of liquid water to the void space of the porous medium. It is controlled by the pressure gradient and the void space of the porous medium [22].

$$\frac{\partial}{\partial t} (\epsilon \rho_l s) = \nabla \cdot \left(\frac{\rho_l K K_r \nabla P_l}{\mu_l} \right) + S_{gl} - S_{ld}, \quad (10)$$

where K is the permeability, S_{gl} is the mass change rate between gas and liquid and S_{ld} is the mass change rate between liquid and dissolved phases.

The generation and transport of dissolved phases are stated as follows [23]:

$$\begin{aligned} \frac{\partial}{\partial t} (\epsilon M_{\text{H}_2\text{O}} \frac{\rho_l}{\text{EW}} \lambda) + \nabla \cdot (\vec{i} \frac{n_d}{F} M) \\ = \nabla \cdot (M D^i \nabla \lambda) + S_\lambda + S_{gd} + S_{ld} \end{aligned} \quad (11)$$

where M is the molecular weight, EW is the equivalent weight of membrane, \vec{i} is the ionic current density, n_d is the osmotic drag coefficient, D^i is the diffusion coefficient, and S_λ is the water production rate of the cathode catalyst layer. Mass change rates of S_{gd} and S_{ld} are defined as [22]:

$$S_{gd} = (1 - s^\theta) \gamma_{gd} M_{\text{H}_2\text{O}} \frac{\rho_l}{\text{EW}} (\lambda_E - \lambda), \quad (12)$$

$$S_{ld} = s^\theta \gamma_{ld} M_{\text{H}_2\text{O}} \frac{\rho_l}{\text{EW}} (\lambda_E - \lambda) \quad (13)$$

where γ_{gd} and γ_{ld} are the mass exchange rates and λ_E is the equilibrium water content. λ is the water content, which is equal to the ratio of the number of water

molecules to the number of sulfonic acid ions, which is obtained by [24]:

$$\lambda = \begin{cases} 0.043 + 17.18a - 39.85a^2 + 36.0a^3 & 0 < a \leq 1 \\ 14.0 + 1.4(a - 1.0) & 1 < a < 3 \\ 16.8 & a > 3 \end{cases} \quad (14)$$

where a is the water activity which is defined as:

$$a = \frac{P_w}{P_{\text{sat}}} + 2s \quad (15)$$

where P_w is water vapor pressure and P_{sat} is water saturation pressure in Pascal, which are calculated as follows:

$$P_w = x_{\text{H}_2\text{O}}P, \quad (16)$$

$$\begin{aligned} \log_{10} \left(\frac{P_{\text{sat}}}{101325} \right) &= -2.1794 + 0.02953(T - 273.17) \\ &\quad - 9.1837 \times 10^{-5}(T - 273.17)^2 \\ &\quad + 1.4454 \times 10^{-7}(T - 273.17)^3, \end{aligned} \quad (17)$$

where $x_{\text{H}_2\text{O}}$ is the mole fraction of water vapor in the gas mixture. The following equation is used to model the formation and transfer of liquid water in the gas channels. In order to control water removal and due to the fact that the presence of water in the flow channel increases the pressure drop, it is very important to consider this phenomenon. Hence we have:

$$\frac{\partial}{\partial t}(\rho_l s) + \nabla \cdot (\rho_l \bar{V}_l s) = \nabla \cdot (D_{\text{liq}} \nabla s) \quad (18)$$

where D_{liq} is the diffusion coefficient of liquid water in flow field channels and \bar{V}_l is the liquid velocity which is considered to be a fraction of the velocity of gas as:

$$\bar{V}_l = x \bar{V}_g. \quad (19)$$

3.2 Boundary conditions

To apply the boundary conditions to the walls, except the inlet and outlet, the conditions of zero flux and no-slip were employed. For anode and cathode inlets, mass flow rate, temperature, and mass fraction of species were determined, and liquid water saturation was considered to be equal to zero. The mass fraction of the species was calculated based on the pressure and relative humidity of the inlet gases, and the atmospheric pressure was used in the outlets. Further, the potential at the anode terminal was set to zero and at the cathode terminal varied from 1.1 V to 0.4 V with a step of 0.05 V.

3.3 Solution method

The numerical solution of equations and boundary conditions mentioned in the previous sections of the present study has been carried out using the finite volume method (FVM) and using ANSYS Fluent 19.2 fuel cell module. After adjusting the parameters related to different fuel cell areas by means of validation and calculating input data, different cases were solved. The SIMPLE algorithm was used for coupling velocity and pressure equations and the Second-Order Upwind method was used for discretization. In addition, the Least Square Cell-based method was adopted to calculate the velocity gradient and secondary diffusion term and to find the scalar values. As well, the convergence criterion in this study considered the equality of anodic and cathodic current density up to 10^{-4} to reach a good accuracy for the solution. Also, the electrochemical properties of the solutions were set based on the validated parameters, the PEMFC working temperature was 70 °C and the anode and cathode stoichiometric ratios were the same and set to 1 for single-phase and 2 for two-phase solutions.

3.4 Evaluation criteria

In many studies, fuel cell performance analysis is performed using evaluation criteria. Such criteria help to better analyze the fuel cell performance and increase the efficiency of systems. First, the following criteria were selected among the state-of-the-art literature, and after describing the corresponding results, were analyzed for different designs.

Shen et al. [5, 25] introduced synergy angle and effective mass transfer coefficient (EMTC). The former says that as the synergy angle between the flow velocity and concentration gradient of the reactants becomes lower than 90° mass transfer is better performed.

$$\cos \gamma = \frac{\vec{u} \cdot \nabla c}{|\vec{u}| \cdot |\nabla c|} \quad (20)$$

where \vec{u} is the velocity and ∇c is the concentration gradient. The latter mentions that when the EMTC, which is obtained by the product of flow velocity and concentration gradient proportional to the membrane, rises, better mass transfer is achieved.

$$\text{EMTC} = \left| v \frac{\partial c}{\partial y} \right| \quad (21)$$

where v is the velocity component proportional to the membrane surface.

Ghanbarian et al. [26] proposed a goal function ψ composed of four intermediate functions to investigate the effect of four parameters of pressure drop, oxygen

content in the catalyst layer, oxygen distribution in the catalyst layer, and the formation of liquid water, simultaneously. The functions have equal weights and the ones with positive and negative effects on ψ are in the numerator and denominator of fractions, respectively.

$$\psi = \frac{0.25}{\psi_1} + 0.25\psi_2 + \frac{0.25}{\psi_3} + \frac{0.25}{\psi_4}. \quad (22)$$

Zeng et al. [27] used objective function J to evaluate the PEMFC performance. This function is the ratio of hydraulic power to electric power in the cathode of a fuel cell, and when its value is minimized, the fuel cell performance is the best:

$$J = k \frac{\Delta P_c \bar{u}_{in,c} A_{ch}}{V_{cell} i_{ave} A_m}, \quad (23)$$

where ΔP_c is the pressure drop of the cathode channel, $\bar{u}_{in,c}$ is the inlet velocity, A_{ch} is the channel area, V_{cell} is the cell volume, i_{ave} is the average current density, A_m is the active area and k is a constant with the value of 10^6 . Azarafza et al. [28] used the uniformity index to compare flow fields in terms of uniformity of different variables on a specific surface. The closer the uniformity index is to 1, the more uniform the distribution of the variable. The integral form of this index is as follows:

$$U_a = 1 - \frac{\int_s |J - J_{avg}| ds}{2 \int_s J_{avg} ds} \quad (24)$$

where ds is the target surface, J is the local value of the variable and J_{avg} is defined as follows

$$J_{avg} = \frac{\int_s J ds}{\int_s ds}. \quad (25)$$

3.5 Mesh independency

In order to compare the designs more accurately, almost the same mesh size was used for different samples, after performing the mesh independency tests. The gridding number and type play an important role in the accuracy of the numerical solution. In the present study, a structured mesh has been used in most of the samples. To increase the simulation accuracy, a finer mesh is used near the catalyst layer surfaces, where the reactions take place. To investigate the results of the independence of the gridding, three different mesh sizes have been produced. As can be seen in Figure 4, the results of the cases with 1330000, 2370000, and 3700000 mesh numbers were almost the same, with a slight error in the case with 1330000 mesh. As a result, to reduce the computational cost and prevent a possible divergence of the solution, the mesh configuration of

the case with 2370000 gridding has been used in this study.

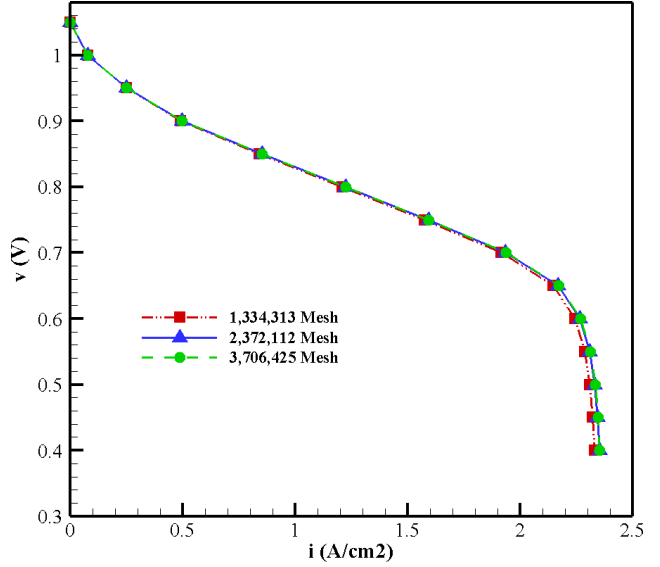


Fig. 4. The polarization curves per the different number of gridding.

3.6 Validation

To validate the configuration and solution methods to reach a precise solution, the validation of this study was performed using data from an experimental study investigating the effect of a new gas flow field on the performance of PEM fuel cells. Then, the numerical simulations were performed after designing, meshing, and setting up the configuration. An overview of the studied design and the comparison between the current densities obtained at different voltages of the present numerical study and those of the reference study is presented in Figure 5.

4 Results and discussion

The performances of different flow fields were investigated in single-phase and two-phase solutions and were compared to each other. Since the pressure drop and water accumulation in cathode flow channels are far more than the anode channels, the affecting parameters are investigated in the cathode.

4.1 Single-phase solution

In this section, first, the results of single-phase simulation were analyzed. Then, to investigate the effects of changes of the desired parameters on the performance of the fuel cell more precisely, a two-phase analysis has been performed which is discussed below.

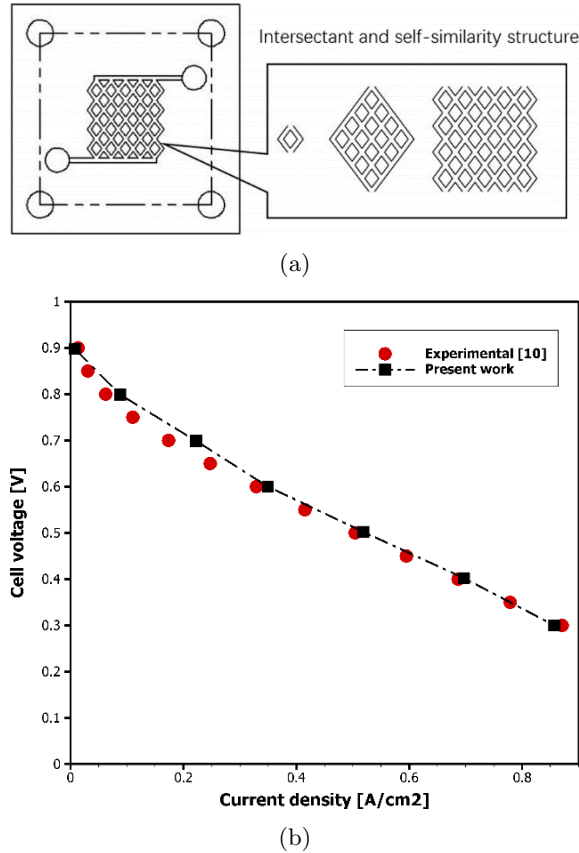


Fig. 5. (a) The experimental design, (b) the comparison of I-V curves of the present numerical study and the reference experimental study [15].

4.1.1 I-V performance

The first parameter studied here is the current density change with voltage, which is introduced in the form of a polarization curve. In general, the polarization curve of PEMFC is divided into three general areas, being respectively affected by activation loss ($V > 0.8$), ohmic loss ($0.6 < V < 0.8$), and concentration loss ($V < 0.6$), respectively. The performance of different flow field designs is compared in Figure 6. As shown in the figure, the main difference of the flow fields is more visible in the end region related to the concentration loss. The best performance among the different designs from the polarization point of view is related to the flow field III and the weakest performance is related to case VII. Field VII, in spite of relatively good performance in the area of concentration loss, has poorer performance than other designs in the area of ohmic loss. In addition, the modified parallel fields (IV and V) show a significant reduction in performance compared to the double channel serpentine designs (I to III). Fields III and II show the best polarization performance, respectively, due to the higher channel surface to the active area as well as the higher velocity in the channel. The

superiority of IV over V at a voltage less than 0.6 V is notable, which shows the good performance of these fields in water purge and better oxygen distribution.

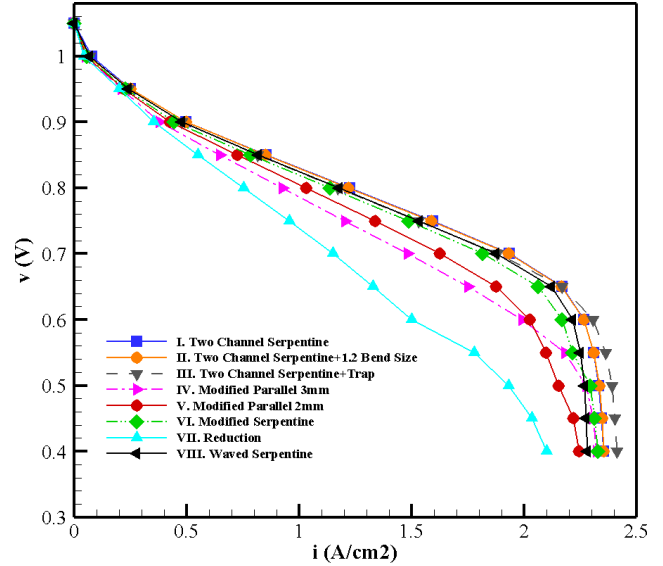


Fig. 6. Comparison of the polarization curve of different flow field designs.

Oxygen distribution One of the main criteria for selecting the appropriate flow field is the distribution of oxygen reactants at the surface of the catalytic layer. The mass fraction of oxygen on the surface of the catalyst layer provides the momentum required for the reaction. If there is more oxygen at this surface, the reaction rate increases, and more current is produced. For this purpose, the selected designs were evaluated from the point of view of the amount and distribution of oxygen concentration on the interface between the gas diffusion layer and the catalyst layer at a voltage of 0.4 V, which is displayed in Figure 7. As can be seen, the oxygen concentration is higher in the inlet sections than the outlets and gradually decreases along the path, which is due to the participation of oxygen in electrochemical reactions and its consumption in the catalyst layer. Additionally, in serpentine bends of different designs, we see an increase in oxygen concentration due to the pressure difference created and also the under rib convection. If the mass fraction of oxygen is low at some points on the catalyst layer, it means that there is a lack of oxygen at those points and it causes the reaction rate to be low, which causes membrane damage in the long run. The higher the oxygen concentration, the lower the risk of oxygen starvation. At a voltage of 0.4 and with more water production in the channels, the performance of different designs in water purge is different and field VII results in the highest oxygen concentration, the reason for which can be the weak participation of oxygen reactants in electrochemical reactions due to the accumulation of moisture.

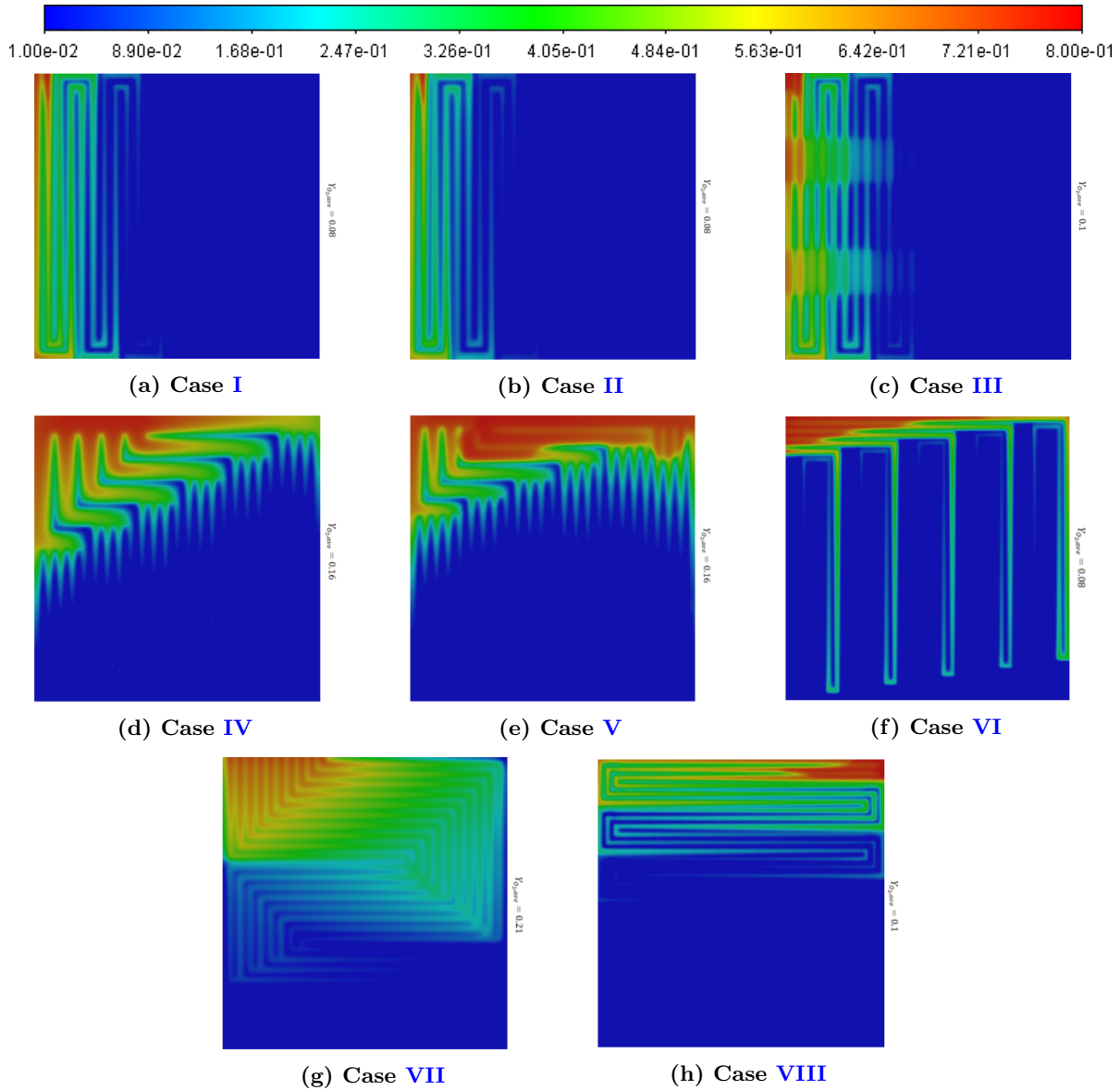


Fig. 7. Oxygen volume fraction at the cathode GDL/CL interface at 0.4 V.

Serpentine designs III and VIII work better at high current densities in the area of concentration loss. At low current densities, however, due to high pumping power, those produce less net power. The pressure drop for these designs, especially design VIII, is very high, although the velocity and mass transfer in the direction perpendicular to the membrane is higher than in other designs. This phenomenon is more discussed in the section of evaluation criteria. Comparing the double-channel serpentine designs (I, II, and III) reveals that with the modifications made, the oxygen distribution becomes more uniform and the part of the flow field with the oxygen concentration less than 5% and the probability of oxygen starvation is reduced. Among

the serpentine designs, channel III has the best performance.

4.1.2 Water activity

Another criterion that can be used to evaluate flow fields is water activity. The solution performed in this section is assumed to be single-phase, so it is not possible to accurately estimate the water content, but the approximate location of the liquid water formation can be predicted. In a single-phase solution, it can be roughly assumed that areas with water activity above 1 represent water production. Figure 8 shows the distribution of water activity at the interface of the cathode GDL and CL for selected designs.

These contours are extracted at 0.4 V. In serpentine designs, more water is produced under the rib, which is due to incomplete water excretion in the serpentine fields. In addition, the better performance of channel III than II and superior performance of that compared to channel I can be obtained from less water activity. On the other hand, field VI due to more paths with lower velocity causes more water accumulation and clogging in the path, which is evidenced by lower oxygen concentrations. The accumulation of water prevents the reactant from flowing and reduces the oxygen concentration. Water control and purging at the output section of the channel are very important.

In the modified parallel models (IV and V), as shown in the figure, the water excretion at the end of the channel is better.

On the other hand, it shows a more uneven distribution than the other designs, which is due to the bigger inlet and outlet cross-sections of the modified parallel designs compared to the rest of the designs. Although the modified parallel fields show less water generation, the double-channel serpentine designs (I, II, and III) show better I-V performance due to the much higher average velocity in the channels (due to the smaller cross-section of inlets).

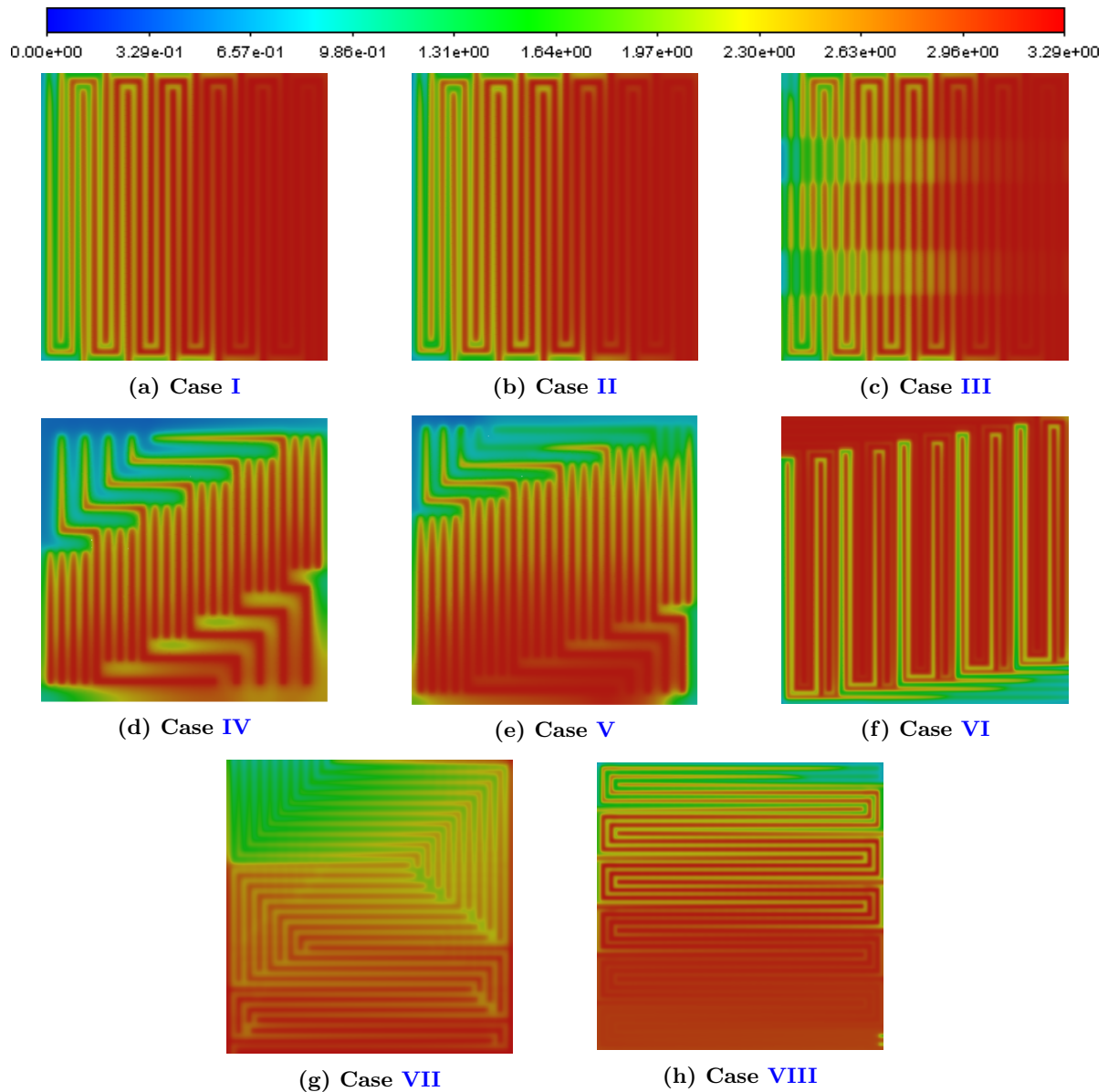


Fig. 8. Water activity at the GDL/CL interface at 0.4 V.

4.1.3 Evaluation criteria

To better analyze the performance of PEMFC, some evaluation criteria are used in the literature. Such criteria help researchers to evaluate the fuel cell performance from other common aspects. To assure the validity of the results, the investigation is performed for two different voltages. Hence, the effect of different designs on goal function, synergy angle and EMTC at 0.7 and 0.4 V are shown in Figures 9 to 11.

Figure 9 shows the goal function index obtained by different flow fields. Since the pressure drop caused by different designs greatly changes from 11 (case IV) to 17147 (case VIII), changes of parameters that consider the pressure drop is dependent on this parameter. Among the studied designs, as expected, the modified parallel designs (IV and V) generate less pressure drop than the other designs due to the nature of parallel flow fields and the larger inlet and outlet cross-sections. This results in achieving the highest value of ψ . On the other hand, flow field VIII experienced the lowest value of ψ due to the very high pressure drop in the flow field. To rank other designs, since the difference between the designs is more significant in the level of pressure drop, the changes of this function have been obtained accordingly and the one with the least pressure drop has achieved the maximum value of ψ .

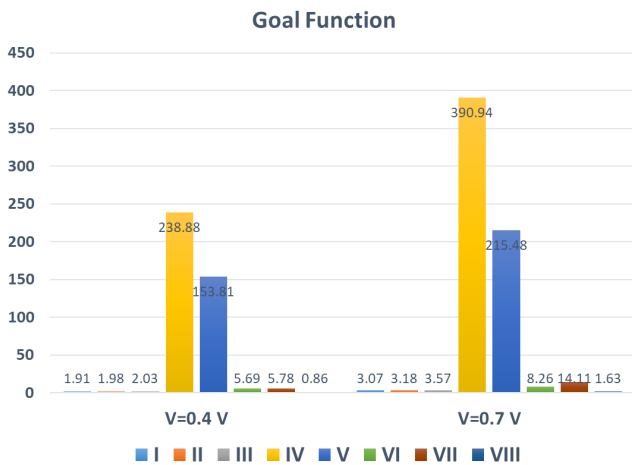


Fig. 9. Goal function variations per different designs at 0.7 V and 0.4 V.

Figure 10 evaluates the synergy angle results. The gas mainstream usually flows perpendicular to the concentration gradient, and a proper mass transfer needs a suitable synergy angle between them. When this factor is reduced, it means that the cell performance has improved. By observing the double-channel designs (I to III), it is observed that fields III and II have a slight advantage over the case I in terms of synergy angle, which corresponds to the results of the polarization

curve. Moreover, the lowest synergy angles obtained are related to the modified parallel fields (IV and V), especially case IV, which happens due to the lower inlet velocity. As mentioned in [25], this factor is not applicable to different types of flow field patterns due to the big difference between the inlet velocities. Besides, cases VI and VII result in better mass transfer and suitable synergy angles due to the continuous transverse changes in the channel path.

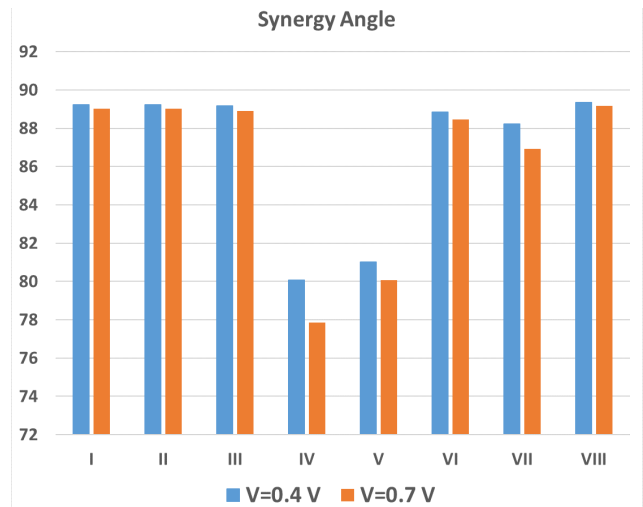


Fig. 10. Synergy angle variations per different designs at 0.7 V and 0.4 V.

Another criterion evaluated here to analyze the performance of the PEM fuel cell is the effective mass transfer coefficient (EMTC), the values of which at voltages of 0.7 V and 0.4 V for different cases are shown in Figure 11. This index examines the mass transfer of the reactants involved in the electrochemical reactions, and the higher the value, the higher the mass transfer rate perpendicular to the membrane plane. It is also affected in some way by the pressure drop, and a flow field with a higher pressure drop experiences better mass transfer perpendicular to the membrane. This phenomenon occurs because when there is a sudden change in direction or channel cross-section, an obstacle is formed in the fluid path and it deviates from its transverse path, leading to higher pressure drop and EMTC. Figure 11 shows that at lower voltages (higher current densities), the EMTC increases due to more mass flow rate, more clogging in the channel path, and greater pressure drop. As for the pressure drop comparison, the highest values of EMTC were achieved by cases VIII and double-channel serpentine designs (II, I, and III), respectively, and the lowest values were obtained by modified parallel designs (IV and V).

As discussed earlier, the uniformity of the distribution of parameters can affect the system performance. Hence, the uniformity index of O₂, current density and

relative humidity distribution on the cathode GDL/CL interface, and temperature distribution on the middle surface of the membrane were compared for different designs.

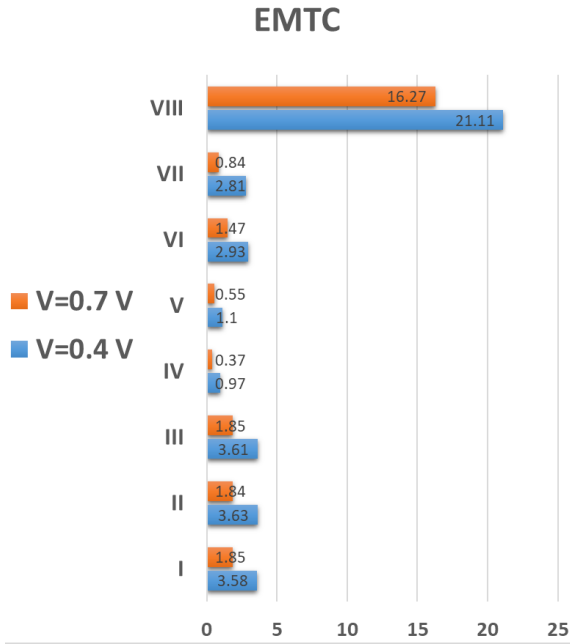


Fig. 11. EMTC variations per different designs at 0.7 V and 0.4 V.

The closer the uniformity index value is to one, the more uniform the distribution of parameters. Figure 12 shows the resulted uniformity indexes for different cases at 0.7 and 0.4 V. The uniformity of O₂, current density, and temperature decrease at lower voltages due to the consumption of oxygen, however, its value for the relative humidity at lower voltages rises since more water is generated at lower voltages and distribute more uniformly. The most uniform case was VII due to less consumption of the reactants and case III showed the second-best results in this section.

4.2 Two-phase solution

4.2.1 Fuel cell performance

In this section, the results of the two-phase solution are presented. In order to better investigate the performance changes, the performance of different cases was obtained for two constant current densities of 0.6 and 2 A/cm². Achieving the desired current density at a higher voltage means better electrical performance.

Figure 13 shows the performance of different cases. The results showed that despite a more accurate analysis by two-phase solution through considering water saturation, the single-phase solution also provides suitable approximate results for comparing different types

of flow fields. At lower current densities (0.6 A/cm²), it was observed that different designs show almost the same performance. However, at higher current densities (2 A/cm²), it was observed that case VIII achieves this current density at a higher voltage, which proves its superiority. The subsequent highest performances were seen by cases I to III with a relative superiority over each other. Moreover, the lowest voltage was obtained by the modified parallel flow fields (IV and V, respectively).

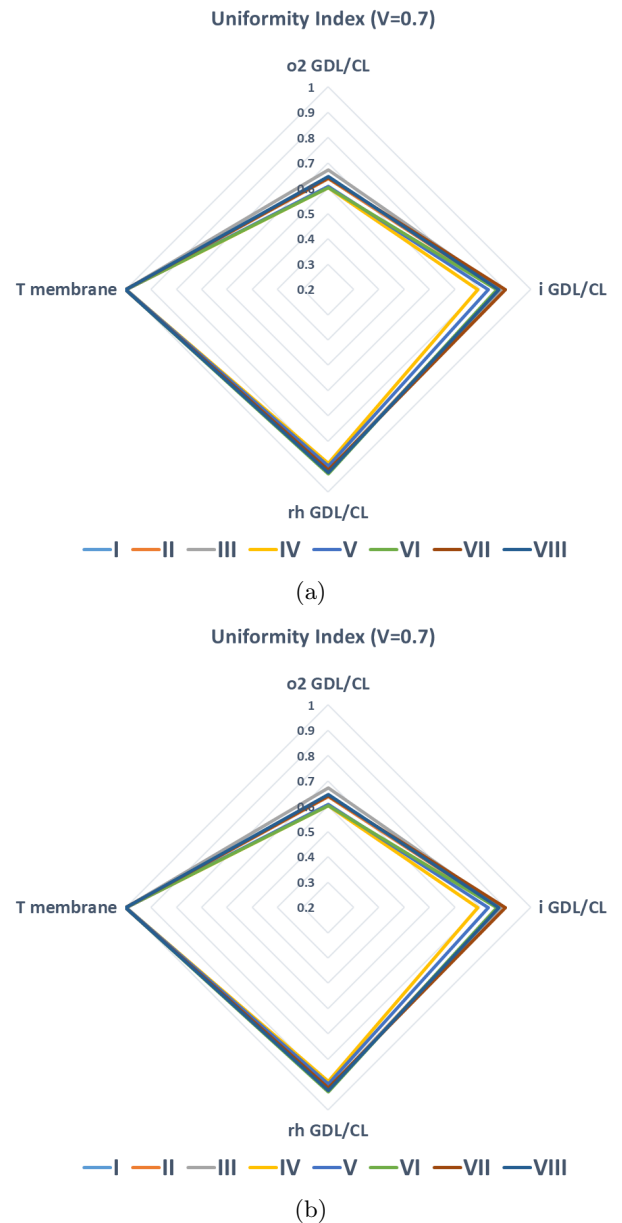


Fig. 12. Uniformity index variations per different designs at: (a) 0.7 V and (b) 0.4 V

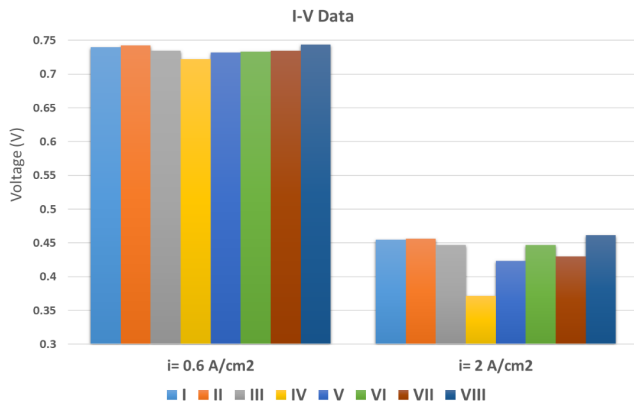


Fig. 13. Electric potential variations per different designs at 0.6 and 2 A/cm².

4.2.2 Oxygen distribution

Figure 14 shows the changes in the oxygen mass fraction for different designs in 2 A/cm² at the interface between the CL and the GDL of the cathode. As mentioned earlier, higher oxygen levels at GDL/CL, especially at higher current densities, can indicate the availability of the reactants to perform the reactions, and this could also mean better overall performance of the fuel cell.

The highest average oxygen mass fraction was obtained by case VIII with the value of 0.75, which is following its better electrical performance. The double-channel serpentine designs (II, I, and III, respectively) show the next highest average oxygen concentration. Also, the lowest oxygen level was obtained by modified parallel designs (IV and V) and reduction (VII).

4.2.3 Current density distribution

To better evaluate the performance of a fuel cell, it is important to study the current density distribution. Figure 15 shows the current density distribution on the cathode GDL/CL interface at voltages of 0.7 and 0.4 V. The uniform distribution of current density prevents the formation of hot spots in the membrane and increases the durability of the membrane. As can be seen, the worst uniformity of the current density distribution is related to cases IV and V, respectively. This phenomenon is due to the wider channel of the modified parallel designs than the serpentine designs, which causes the current density to increase underneath the flow path and to produce less current density in the under rib areas.

Comparing the current density contours at voltages of 0.7 and 0.4 V, it can be concluded that at lower voltages, the uniformity of the current density is disturbed due to the generation of water in the channel path and the reduction of oxygen concentration.

4.2.4 Water saturation

Figure 16 shows the distribution of water saturation in the cathode catalyst layer for selected flow fields. Since flooding and water saturation usually occur at higher current densities due to the increase in reaction rate and water content, the contours are obtained for a current density of 2 A/cm². As seen, in serpentine channels, more water saturation occurs under the rib due to an incomplete purge of water there compared to the channel path. Case VIII increases the oxygen concentration to GDL due to periodic changes of the channel depth that moves water under the rib to flow in the channel. Therefore, the reactants flow prevents the accumulation of water and results in a more uniform distribution. In addition, the inlet and outlet cross-section areas of the cases affect the level of pressure drop and water purge, and generally, pressure drop helps water to be purged. Due to the larger inlet and outlet cross-sections of the modified parallel designs (IV and V), the lower average water is generated in the CL of these cases than those of the other cases. Case VII faces the flooding problem due to having only one outlet against 10 inlets, which is shown by the clogs created in Figure 14g. Although cases VI and VII have almost similar performances in other aspects, case VI results in better water dissipation due to having more outlets.

4.2.5 Evaluation criteria

The effects of different flow field designs on fuel cell performance from the prospects of EMTC and objective function in 0.6 and 2 A/cm² are shown in Figures 16 and 17. As stated, a higher value of EMTC indicates better mass transfer in the direction perpendicular to the membrane. In a two-phase solution, it was observed that this index is the closest criterion to the electrical performance of cases. EMTC variations caused by pressure drop changes due to the type of designs (serpentine or parallel) are also visible here. Figure 17 shows that case VIII also results in a higher value of EMTC, followed by double-channel designs (III, II, and I, respectively). Further, the lower EMTC of parallel designs (IV and V) here indicates weaker mass transfer due to the wider channels and larger inlet and outlet cross-sections.

On the other hand, Figure 18 shows the changes in the objective function for different cases. The obtained results for current densities turned out to be 0.6 and 2 A/cm². As stated, the objective function shows the ratio of hydraulic power to the electrical power at the cathode, and its lower values indicate better efficiency. Since the difference between the pressure drop caused by different designs is much greater than the

changes in their electrical performance, the changes in the resulted objective functions are a function of the pressure drop level. As it was observed, designs VIII, III, I, and II generate the highest pressure drop, respectively. This factor also indicates that more pres-

sure drop means more hydraulic power consumption and therefore a higher objective function, which is not desired. Parallel designs (IV and V) achieve the best results here.

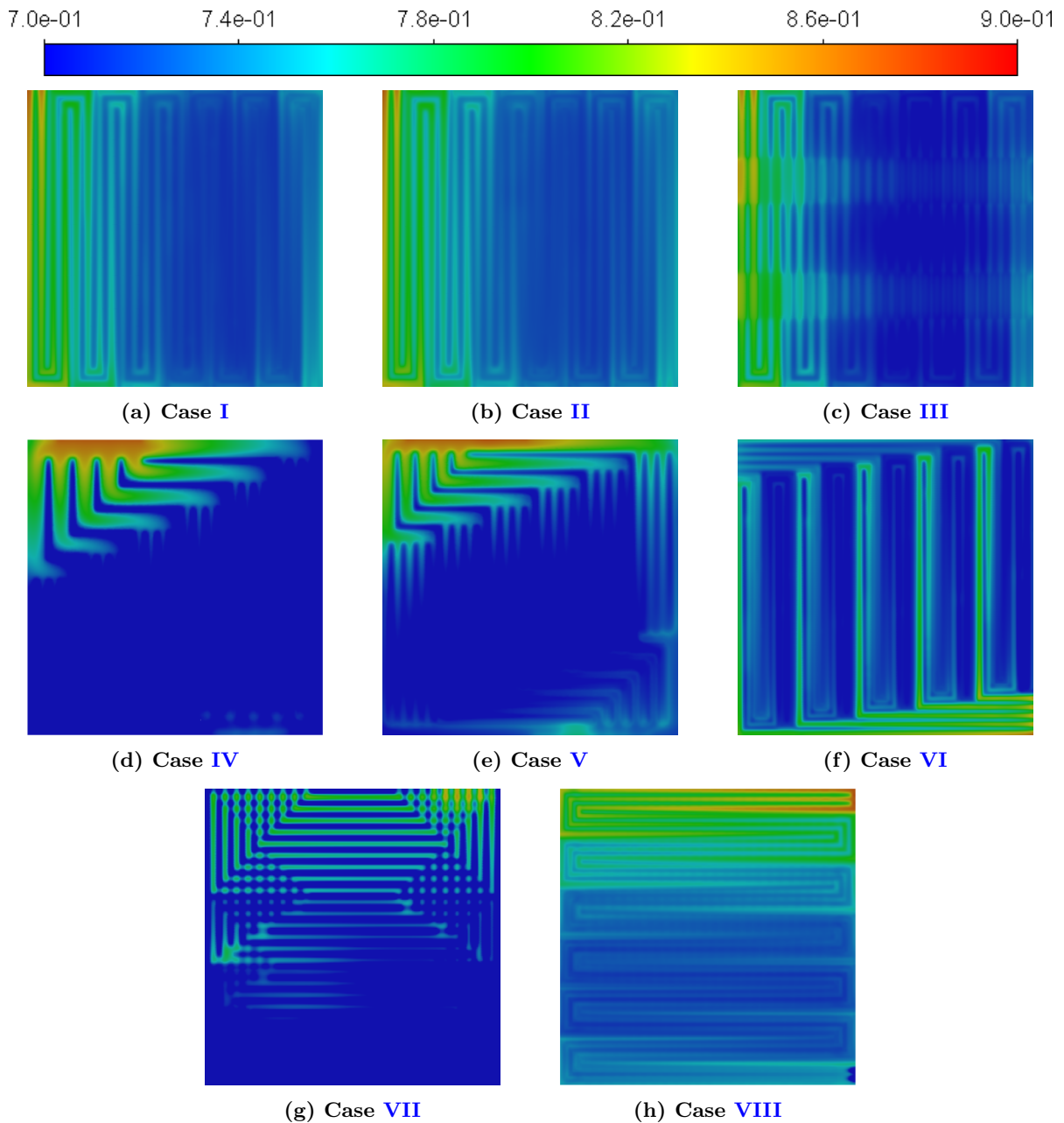


Fig. 14. Oxygen volume fraction at the cathode GDL/CL interface at 2 A/cm^2 .

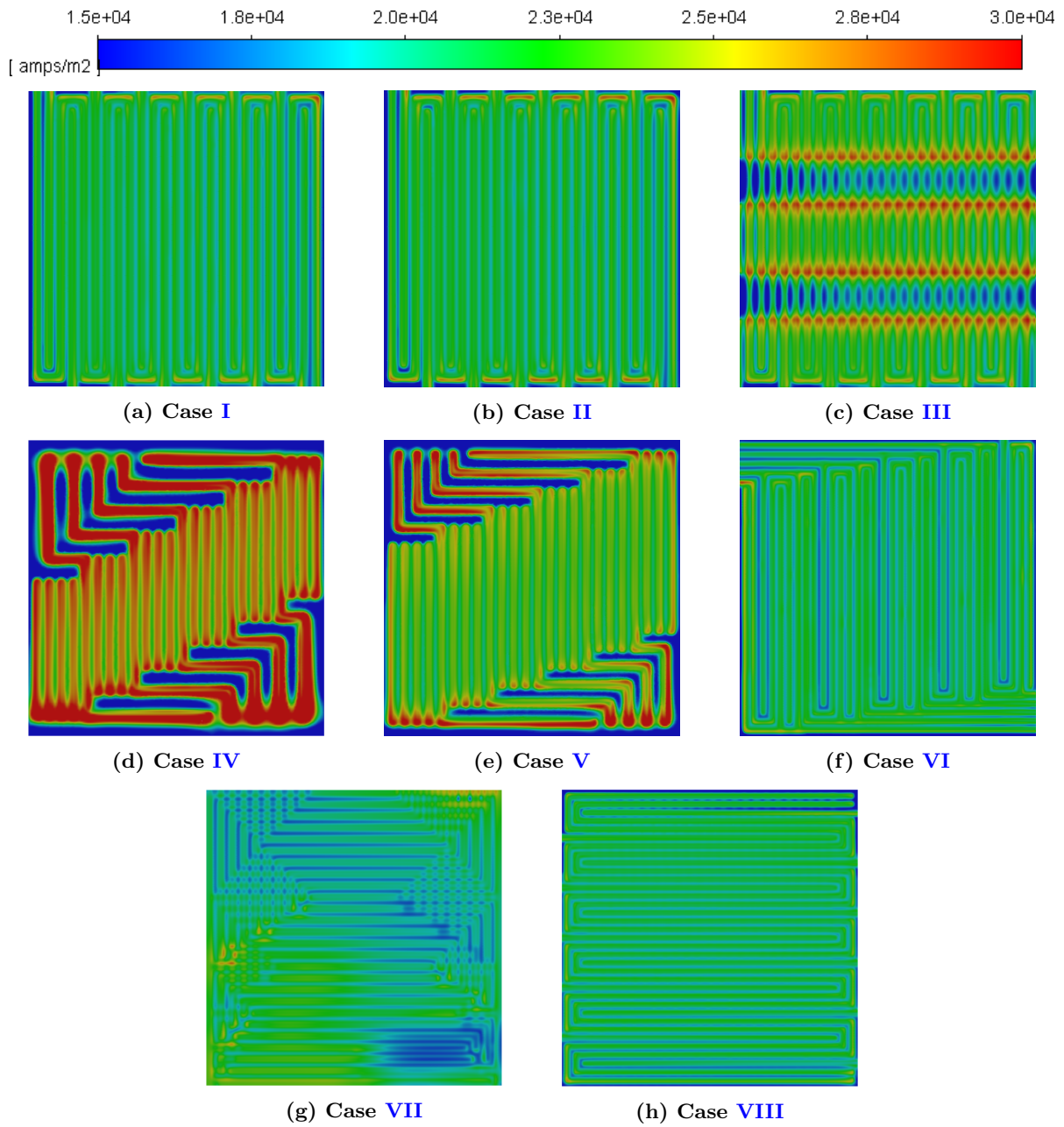


Fig. 15. Current density distribution at the cathode GDL/CL interface at 2 A/cm^2 .

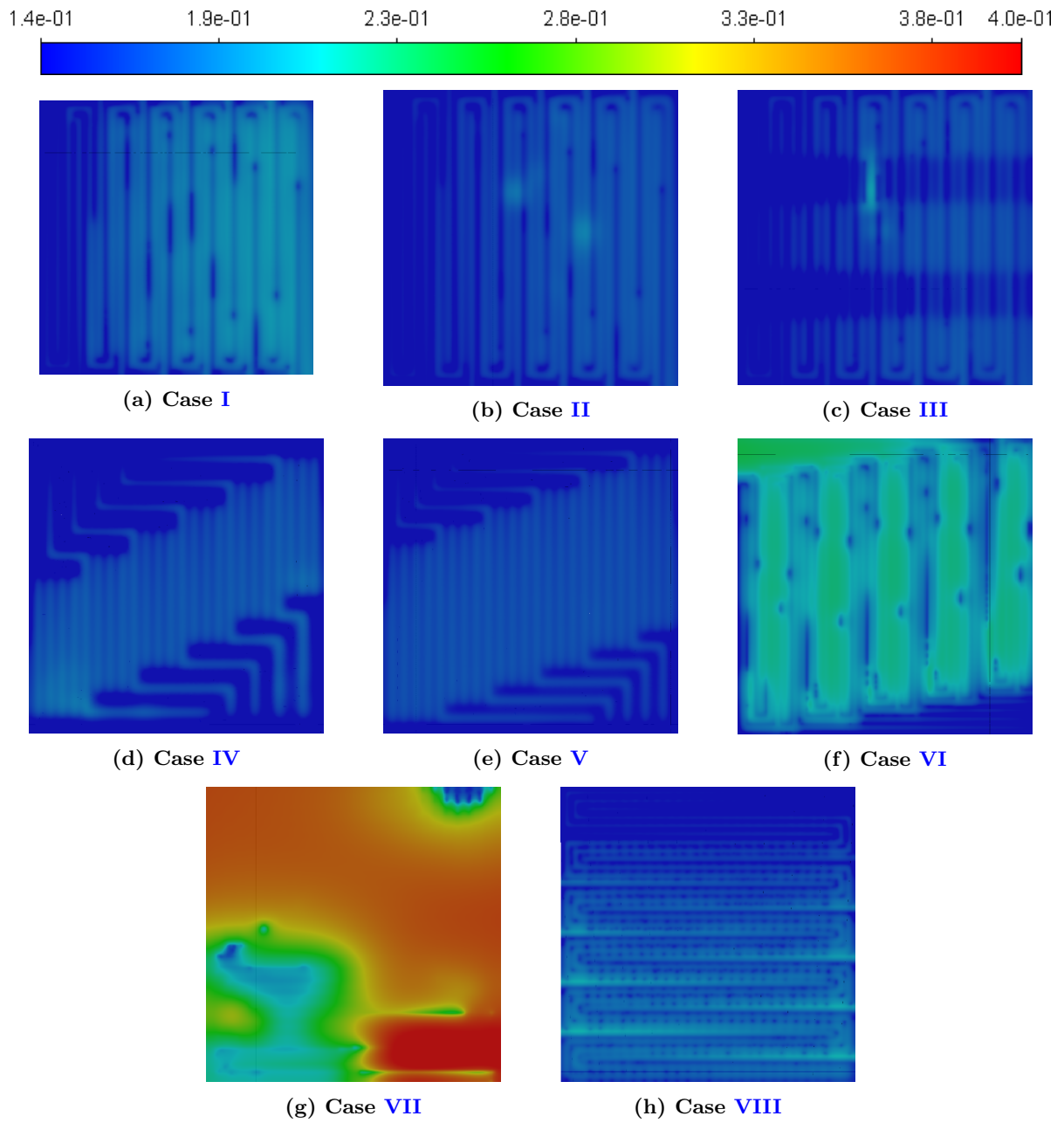


Fig. 16. Water saturation in the cathode catalyst layer at 2 A/cm^2 .

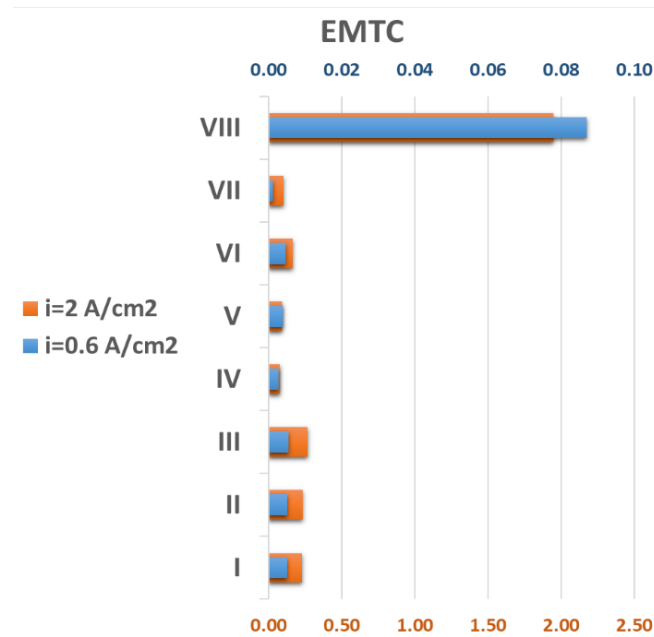


Fig. 17. EMTC in the cathode channel at 0.6 and 2 A/cm².

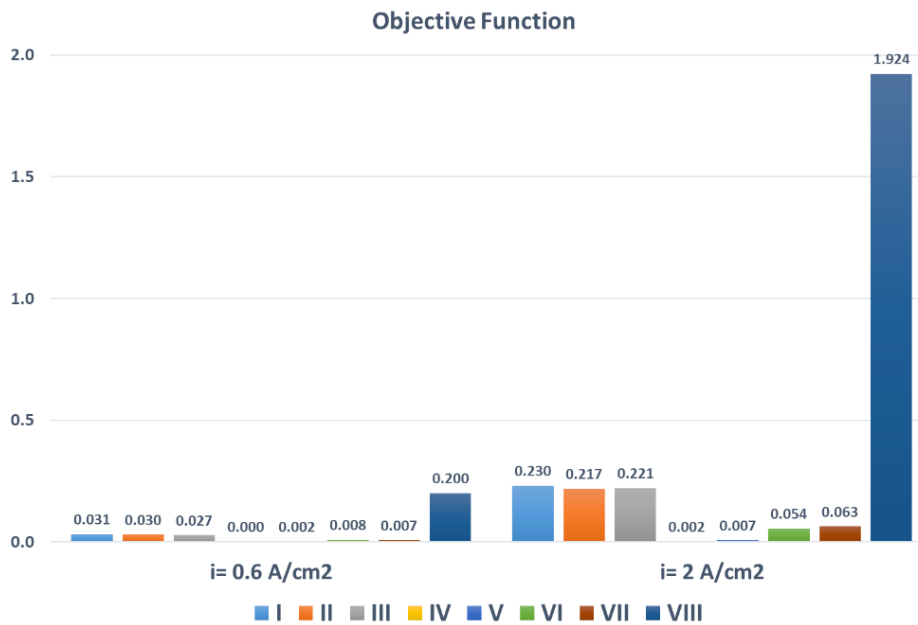


Fig. 18. The objective function in the cathode channel at 0.6 and 2 A/cm².

Figure 19 displays the synergy angle results of different designs by two-phase solution. By observing the double-channel designs (I to III) at 2 A/cm², it is found that case III has a slight advantage over case II and that over the case I in terms of synergy angle, which corresponds to the results of the single-phase synergy angle analysis.

Also, modified parallel cases (IV and V) showed the best results here with the lowest synergy angle, espe-

cially case IV because of the far lower inlet velocity. As discussed earlier, this factor is not applicable to different types of flow field patterns due to the big difference between the inlet velocities.

4.2.6 Performance Factor (PF)

The abovementioned criteria were evaluated to compare and rank different designs. The results showed

that only a few criteria only in some cases could rank the investigated designs. Hence, it is tried to define a new factor to help users rank the best flow field patterns out of different ones.

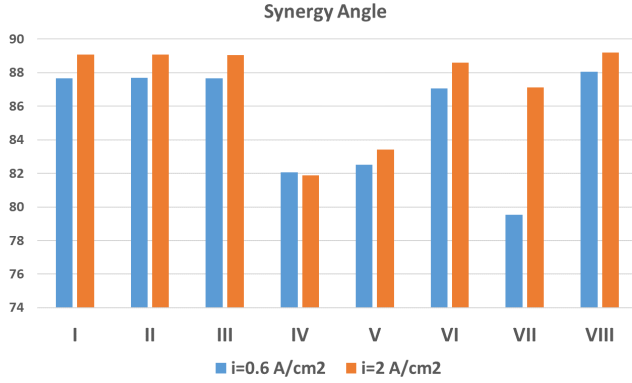


Fig. 19. Synergy angle in the cathode channel at 0.6 and 2 A/cm².

A new criterion named Performance Factor (PF) is introduced here for this purpose. It consists of four parameters with the same weights: O₂ average on GDL/CL, inlet velocity U_{in} , UI of O₂, i and water saturation on GDL/CL, and EMTC in the cathode channel.

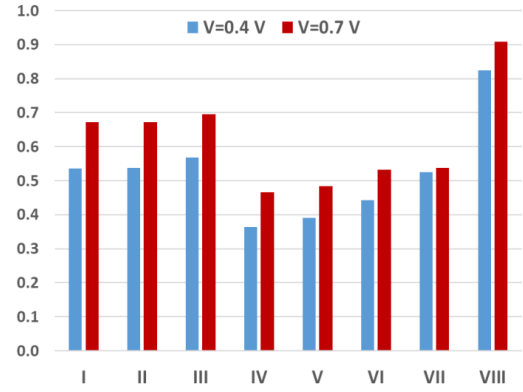
$$\begin{aligned}
 PF = & 0.25 (O_2)_{ave} + 0.25 \frac{U_{in}}{U_{in,max}} \\
 & + 0.25 \left(\frac{UI_{O_2} + UI_i + UI_{water}}{3} \right) \\
 & + 0.25 \frac{EMTC_{cathode}}{EMTC_{max}} \quad (26)
 \end{aligned}$$

Evaluating the PF showed that it could be a useful tool to rank different cases. As can be seen in Figure 20, the obtained results in single-phase and two-phase analyses are very close to the rankings achieved by the I-V performances which shows the applicability of this factor. As for the polarization results, the worst performances were resulted by cases IV and V, respectively, and the best performance was achieved by case VIII. Besides, the comparison of the double-serpentine cases (I to III) was very close to the electrical performance ranking of the pattern. The results showed that this factor could be used as a suitable criterion when comparing different flow field patterns.

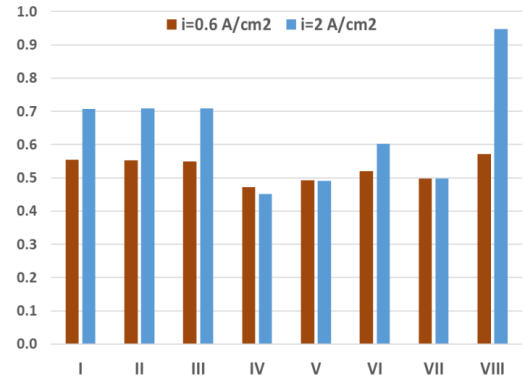
5 Conclusions

In this study, the effect of different flow fields on the performance of PEM fuel cells was investigated using computational fluid dynamics. Additionally, the performances of flow field designs have been evaluated with

the help of new evaluation criteria. First, a fuel cell was simulated to verify the accuracy of the solution, and the results of the polarization curve were accurately validated by an experimental study.



(a) single-phase



(b) single-phase

Fig. 20. Performance factor variations of different cases in: (a) single-phase, (b) two-phase analyses

Then, by reviewing the literature and analyzing the results, some flow field designs inspired by novel works were presented and compared to some superior designs from previous studies. In addition to analyzing efficient evaluation criteria, a novel factor was produced with the best agreement with the PEM performance. To investigate more comprehensively, the simulations were performed in single-phase and two-phase approaches, and the results were compared. The following conclusions could be drawn.

- Observing the polarization curves obtained from different flow fields indicated that the double-channel serpentine designs (III, II, and I, respectively) and case VIII showed the best performances overall.
- Although the modified parallel flow fields (IV and V) showed the best performances in water purge and pressure drop, the I-V performance was almost the worst.

- By studying the results of evaluation criteria and polarization curves, it was observed that serpentine cases compared to parallel ones lead to the higher output power due to more mass flow rate of the reactants in the channels and better mass transfer of reactants.
- The two-phase study revealed that the waved serpentine case has the highest electrical performance with the highest mass fraction of oxygen. In addition, the EMTC evaluation showed that this factor is in almost accordance with the electrical performance of different cases.
- The analyses of evaluation criteria showed that the factors that are directly dependent on the pressure drop are not applicable when comparing different types of flow field patterns. Because the difference between the pressure drop values is very significant.
- Although the two-phase analysis is more concise and consistent with the other obtained results, the single-phase analysis which is computationally cost-effective can predict the performance of different types of flow field patterns, especially at higher voltages.
- A new parameter (Performance Factor) was introduced here that showed a successful performance in ranking different flow field patterns. It was used for single-phase and two-phase analyses and the results were very close to the obtained electrical performance.

Nomenclature

a	The active area (1/m)
C	Concentration
D_w^i	Diffusion coefficient
e	Electron
F	Faraday's constant (C/mol)
H	Hydrogen
i	Current density (A/cm ²)
j_{an}^{ref}	The reference exchange current density at the anode (A/m ²)
j_{cat}^{ref}	The reference exchange current density at the cathode (A/m ²)
k	Thermal conductivity (W/mK)
M_i	Molecular mass of species (kg/mol)
n_d	Electroosmotic drag coefficient
P_l	Liquid pressure
R	Universal gas constant (j/mol.K)
RH	Relative humidity
s	Saturation
S	Source term
S_{gl}	The rate of mass change between gas and liquid phase

S_{ld}	The rate of mass change between liquid and dissolved phase
T	Temperature (K)
V	Voltage (V)

Greek symbols

α	Anode transfer coefficient
β	Cathode transfer coefficient
ϵ	Porosity
η	The overpotential (V)
λ	Water content
σ	The electric conductivity (1/ohm · m)
μ	Dynamic viscosity (kg/m ² s)
ρ	Density (kg/m ² s)

Superscript and subscript

a	Anode
c	Cathode
l	Liquid
g	Gas
s	Solid
mem	Membrane

Abbreviations

GDL	Gas diffusion layer
CL	Catalyst layer
PEMFC	EMTC Polymer electrolyte membrane fuel cell
EMTC	Effective mass transfer coefficient

References

- [1] Manso A, Marzo F, Barranco J, Garikano X, Mujika MG. Influence of geometric parameters of the flow fields on the performance of a PEM fuel cell. A review. International journal of hydrogen energy. 2012;37(20):15256–15287.
- [2] Kahraman H, Orhan MF. Flow field bipolar plates in a proton exchange membrane fuel cell: Analysis & modeling. Energy Conversion and Management. 2017;133:363–384.
- [3] Lim B, Majlan E, Daud W, Husaini T, Rosli MI. Effects of flow field design on water management and reactant distribution in PEMFC: a review. Ionics. 2016;22:301–316.
- [4] Lim B, Majlan E, Daud W, Rosli M, Husaini T. Numerical investigation of the effect of three-dimensional modified parallel flow field designs on proton exchange membrane fuel cell performance. Chemical Engineering Science. 2020;217:115499.

- [5] Shen J, Tu Z, Chan SH. Enhancement of mass transfer in a proton exchange membrane fuel cell with blockage in the flow channel. *Applied Thermal Engineering*. 2019;149:1408–1418.
- [6] Rostami L, Nejad PMG, Vatani A. A numerical investigation of serpentine flow channel with different bend sizes in polymer electrolyte membrane fuel cells. *Energy*. 2016;97:400–410.
- [7] Ramin F, Sadeghifar H, Torkavannejad A. Flow field plates with trap-shape channels to enhance power density of polymer electrolyte membrane fuel cells. *International Journal of Heat and Mass Transfer*. 2019;129:1151–1160.
- [8] Singdeo D, Dey T, Gaikwad S, Andreasen SJ, Ghosh PC. A new modified-serpentine flow field for application in high temperature polymer electrolyte fuel cell. *Applied energy*. 2017;195:13–22.
- [9] Baz F, Ookawara S, Ahmed M. Enhancing under-rib mass transport in proton exchange membrane fuel cells using new serpentine flow field designs. *International Journal of Hydrogen Energy*. 2019;44(58):30644–30662.
- [10] Alizadeh E, Rahimi-Esbo M, Rahgoshay S, Saadat S, Khorshidian M. Numerical and experimental investigation of cascade type serpentine flow field of reactant gases for improving performance of PEM fuel cell. *International Journal of Hydrogen Energy*. 2017;42(21):14708–14724.
- [11] Li W, Zhang Q, Wang C, Yan X, Shen S, Xia G, et al. Experimental and numerical analysis of a three-dimensional flow field for PEMFCs. *Applied Energy*. 2017;195:278–288.
- [12] Ashrafi M, Kanani H, Shams M. Numerical and experimental study of two-phase flow uniformity in channels of parallel PEM fuel cells with modified Z-type flow-fields. *Energy*. 2018;147:317–328.
- [13] Heidary H, Kermani MJ, Advani SG, Prasad AK. Experimental investigation of in-line and staggered blockages in parallel flowfield channels of PEM fuel cells. *International journal of hydrogen energy*. 2016;41(16):6885–6893.
- [14] Heidary H, Kermani MJ, Dabir B. Influences of bipolar plate channel blockages on PEM fuel cell performances. *Energy Conversion and Management*. 2016;124:51–60.
- [15] Wen Dh, Yin LZ, Piao Zy, Li G, Leng Qh, et al. Performance investigation of proton exchange membrane fuel cell with intersectant flow field. *International Journal of Heat and Mass Transfer*. 2018;121:775–787.
- [16] Beattie PD, Basura VI, Holdcroft S. Temperature and pressure dependence of O₂ reduction at Pt / Nafion® 117 and Pt/ BAM® 407 interfaces. *Journal of Electroanalytical Chemistry*. 1999;468(2):180–192.
- [17] Khandelwal M, Mench M. Direct measurement of through-plane thermal conductivity and contact resistance in fuel cell materials. *Journal of Power Sources*. 2006;161(2):1106–1115.
- [18] Nguyen TV, White RE. A water and heat management model for proton-exchange-membrane fuel cells. *Journal of the Electrochemical Society*. 1993;140(8):2178.
- [19] Wang XD, Zhang XX, Yan WM, Lee DJ, Su A. Determination of the optimal active area for proton exchange membrane fuel cells with parallel, interdigitated or serpentine designs. *International Journal of Hydrogen Energy*. 2009;34(9):3823–3832.
- [20] Springer TE, Zawodzinski T, Gottesfeld S. Polymer electrolyte fuel cell model. *Journal of the electrochemical society*. 1991;138(8):2334.
- [21] Mann R, Amphlett J, Peppley B, Thurgood C. Application of Butler–Volmer equations in the modelling of activation polarization for PEM fuel cells. *Journal of power sources*. 2006;161(2):775–781.
- [22] Pasaogullari U, Wang CY. Two-phase transport and the role of micro-porous layer in polymer electrolyte fuel cells. *Electrochimica Acta*. 2004;49(25):4359–4369.
- [23] Wu H, Li X, Berg P. On the modeling of water transport in polymer electrolyte membrane fuel cells. *Electrochimica Acta*. 2009;54(27):6913–6927.
- [24] Maggio G, Recupero V, Mantegazza C. Modelling of temperature distribution in a solid polymer electrolyte fuel cell stack. *Journal of Power Sources*. 1996;62(2):167–174.
- [25] Shen J, Tu Z, Chan SH. Evaluation criterion of different flow field patterns in a proton exchange membrane fuel cell. *Energy conversion and management*. 2020;213:112841.
- [26] Ghanbarian A, Kermani MJ, Scholta J, Abdollahzadeh M. Polymer electrolyte membrane fuel

cell flow field design criteria—application to parallel serpentine flow patterns. *Energy conversion and management*. 2018;166:281–296.

[27] Zeng X, Ge Y, Shen J, Zeng L, Liu Z, Liu W. The optimization of channels for a proton exchange membrane fuel cell applying genetic algorithm.

International journal of heat and mass transfer. 2017;105:81–89.

[28] Azarafza A, Ismail MS, Rezakazemi M, Pourkashanian M. Comparative study of conventional and unconventional designs of cathode flow fields in PEM fuel cell. *Renewable and Sustainable Energy Reviews*. 2019;116:109420.